The Astrophysical Journal, 629:239–249, 2005 August 10

NGC 300: AN EXTREMELY FAINT, OUTER STELLAR DISK OBSERVED TO 10 SCALE LENGTHS

J. Bland-Hawthorn
Anglo-Australian Observatory, P.O. Box 296, Epping, NSW 2121, Australia

M. Vlajić
Anglo-Australian Observatory, P.O. Box 296, Epping, NSW 2121, Australia

K. C. Freeman
Mount Stromlo Observatory, Private Bag, Woden, ACT 2611, Australia

and

B. T. Draine
Princeton University Observatory, Princeton University, Peyton Hall, Princeton, NJ 08544-1001
Received 2004 November 11; accepted 2005 March 22

ABSTRACT

We have used the Gemini Multi-Object Spectrograph (GMOS) on the Gemini South 8 m telescope in exceptional conditions (0.″6 FWHM seeing) to observe the outer stellar disk of the Sculptor Group galaxy NGC 300 at two locations. At our point-source detection threshold of $r' = 27.0$ (3 σ) mag, we trace the stellar disk out to a radius of 24′, or $2.2R_{25}$, where R_{25} is the 25 mag arcsec^{-2} isophotal radius. This corresponds to about 10 scale lengths in this low-luminosity spiral galaxy ($M_B = -18.6$), or about 14.4 kpc at a Cepheid distance of 2.0 ± 0.07 Mpc. The background galaxy counts are derived in the outermost field, and these are within 10% of the mean survey counts from both Hubble Deep Fields. The luminosity profile is well described by a nucleus plus a simple exponential profile out to 10 optical scale lengths. We reach an effective surface brightness of $\mu_{r'} =$ 30.5 mag arcsec^{-2} (2 σ) at 55% completeness, which doubles the known radial extent of the optical disk. These levels are exceedingly faint in the sense that the equivalent surface brightness in B or V is about 32 mag arcsec^{-2}. We find no evidence for truncation of the stellar disk. Only star counts can be used to reliably trace the disk to such faint levels, since surface photometry is ultimately limited by nonstellar sources of radiation. In the Appendix, we derive the expected surface brightness of one such source: dust scattering of starlight in the outer disk.

Subject headings: galaxies: individual (NGC 300) — galaxies: stellar content — galaxies: structure

1. INTRODUCTION

The structure of the outer parts of galactic disks is central to our understanding the formation and evolution of spiral galaxies. The surface brightness profile of a spiral galaxy is a first-order signature of the formation process (Freeman & Bland-Hawthorn 2002; van der Kruit 1987; Ferguson & Clarke 2001). By measuring scale lengths for galaxy samples of different redshifts, it is, for example, possible to directly address the evolution of galactic disks (Labbé et al. 2003).

To a first approximation, the radial light distribution of disks is well described by an exponential decline (Freeman 1970). If the exponential is due to dynamical evolution (Lin & Pringle 1987), it is important to establish out to what radius this process took place. It is possible that departures from an exponential will show up at faint levels, reflecting new forms of dynamical evolution or different angular momentum of the outermost accreted material.

Previous studies have shown that the exponential light distribution breaks smoothly at a well-defined "break radius" in some galaxies (Pohlen et al. 2002; de Grijs et al. 2001). In the optical, this occurs at galactocentric distances of typically 3–5 exponential scale lengths. In principle, this break radius could be used as an intrinsic parameter to measure the size of a galactic disk. However, despite the fact that these breaks have been known for more than 20 years (van der Kruit 1979), we do not have a secure understanding of the origin of the break, so their application as a fundamental disk characteristic is therefore not yet possible.

Beyond the break radius, stars are detected, albeit with a steeply declining luminosity profile (e.g., Kregel et al. 2002). To date, the outer edge of the stellar disk ("truncation radius") has not been detected in any galaxy, largely because diffuse light photometry is unreliable at such faint magnitude limits. We note in two previous papers that optical disks are seen to extend to 10 optical scale lengths. In their study of NGC 5383, Barton & Thompson (1997) reach down to almost $\mu_V \approx 30$ mag arcsec^{-2} (1 σ). In a multiband study of NGC 4123, Weiner et al. (2001) reach 29, 29, and 28 mag arcsec^{-2} (1 σ) in B, V, and I, respectively. However, we point out that both of these galaxies are strongly barred and have peculiar morphologies.

We choose to focus our first study of outer disks on the Sculptor Group for several reasons. It is the closest galaxy group to the Local Group with a high proportion of disk systems. Furthermore, the group has not undergone much dynamical evolution—the galaxies are more or less isolated. Their dark halos are thought to extend far beyond the bright disks. In principle, accretion onto the halo could give rise to disks that are much larger than normally assumed.

The layout of the paper is as follows. Our motivation for targeting NGC 300 is discussed in § 2. We briefly discuss surface photometry versus star counts in § 3 and show that the latter is the only way to get below 30 mag arcsec^{-2} reliably, an issue we return to in the Appendix. The observations and reductions under

IRAF are discussed in § 4, while details of the photometric calibration are given in § 5. The results are presented in § 6, and these are discussed in § 7.

2. OBJECT SELECTION

We chose NGC 300 as a relatively undisturbed member of the closest galaxy group, Sculptor. NGC 300 lies at the near side of a distribution that is elongated along the line of sight (Jerjen et al. 1998). There have been various distance estimates based on Cepheid variables (Freedman et al. 2001; Gieren et al. 2004) and the tip of the red giant branch (Butler et al. 2004). We adopt a weighted mean of 26.5 ± 0.1 for the distance modulus, equivalent to 2.0 ± 0.1 Mpc. We show below that our photometry reaches down to an intrinsic stellar magnitude of $M_r' = 0.5$ (3 σ), which includes some of the giant branch and much of the horizontal branch in a moderately metal-poor ([Fe/H] ≈ -1) population.

The late-type spiral galaxy NGC 300 is ideal for our proposed study. It is an almost pure disk galaxy (bulge light <2%) and has a mild inclination ($i = 42°$). The galaxy lies at high Galactic latitude ($b \approx -79°$) and therefore has a low foreground reddening of $E(B-V) = 0.013$ mag. NGC 300 shares important similarities with M33 in the northern hemisphere (Blair & Long 1997). The optical disk scale length has been measured as 2.17 kpc in B_J (Carignan 1985; scaled to a distance of 2.0 Mpc) and 1.47 kpc in I (Kim et al. 2004). We note that these scale lengths would indicate that the color of the outer disk is likely to be very blue, but this has not been measured to date (see § 7). Carignan's (1985, Fig. 8) photometric study reveals that the outermost contours are well behaved, with minimal asymmetry.

3. SURFACE PHOTOMETRY VERSUS STAR COUNTS

There are two basic methods for detecting the faint outer reaches of galaxies: deep diffuse light imaging (e.g., de Vaucouleurs & Capaccioli 1979) and faint star counts (e.g., Pritchet & van den Bergh 1994).

Surface photometry of face-on galaxies provides radial information that is more easily interpreted but is limited by the brightness of the night sky. Edge-on galaxies are the easiest to search for optical breaks and truncations because of the enhanced surface brightness from the line-of-sight integration. However, with edge-on systems one cannot be sure that the surface photometry is not affected by smaller scale structures in the disk, like faint spiral arms, for example, which might mimic the effects of truncation (Pohlen et al. 2004). Dust extinction is also more severe in edge-on systems although less so at large radii.

While diffuse light imaging is a direct method, there are many technical difficulties at levels below $\mu_R \approx 27$ mag arcsec^{-2}. These include scattered light internal to the optics, difficulties in flat-fielding data (Pohlen et al. 2002), zodiacal light (Bernstein et al. 2002), and diffuse Galactic light (Haikala & Mattila 1995), a combination of dust-scattered starlight, dust luminescence, and emission from cool gas. Over the sky, there are also variations in Galactic cirrus (Schlegel et al. 1998) and warm ionized gas due to the Reynolds layer (Reynolds 1992). At fainter levels, in the range $\mu_R \approx 30$–32 mag arcsec^{-2}, the outer H I envelope may have (1) a sufficient column of dust to scatter detectable levels of starlight from the optical disk (see the Appendix) or (2) sufficient levels of ionization due to a local or global radiation field to produce fluorescent emission (Maloney 1993; Maloney & Bland-Hawthorn 2001).

A more powerful method is to count individual stars in the old stellar population. The technique is particularly effective, since good seeing allows contamination from background galaxies and foreground stars to be properly evaluated. In their study of the M31 halo [$(m-M)_o \approx 24.5$], Pritchet & van den Bergh (1994) achieved 50% completeness for point sources down to $V = 24.5$ in 1″ seeing. This corresponds to an "effective" surface brightness limit of $\mu_V = 29$ mag arcsec^{-2} after correcting for foreground contamination and the stellar disk contribution from unresolved stars. With their 4 m ground-based observations, Pritchet & van den Bergh reach $M_V \approx 0$, corresponding to roughly 40% of starlight from the old stellar population. More recently, very deep *Hubble Space Telescope* observations reach $m_I = 31$ at 50% completeness in a relatively small 3′ field (Brown et al. 2003).

With stellar photometry, we can trace the disk to much fainter effective surface brightnesses by resolving individual stars. This is the motivation for our deep GMOS observations. It is, however, crucial to establish the magnitude completeness limit and the fraction of missing light below the detection limit, which we discuss.

TABLE 1
GMOS Observing Log

Target	α (J2000)	δ (J2000)	Date	Exposure (s)
Field 1	00 55 50	−37 47 20	2003 Dec 20–22	9 × 900
Field 2	00 56 15	−37 46 49	2003 Dec 23–26	9 × 900
Landolt 95	03 53 01	+00 00 13	2003 Dec 20	2 × 1.5
	...	...	...	2 × 3.5
Landolt 98	06 51 50	−00 21 17	2003 Dec 21–24	2 × 1.5
	...	...	...	2 × 3.5

Notes.—The Landolt stars are photometric standards discussed in Landolt (1992). Units of right ascension are hours, minutes, and seconds, and units of declination are degrees, arcminutes, and arcseconds.

4. OBSERVATIONS AND DATA REDUCTION

Deep r' images of NGC 300 were obtained in two outer locations using the Gemini Multi-Object Spectrograph (GMOS) on Gemini South during semester 2003 December. The two GMOS fields lie close to the major axis of NGC 300 and span a major axis distance range of 7–16 kpc. Our science goal was to track the radial profile of the galaxy as far as possible, which required the best possible observing conditions. Of the available filter sets, the r' filter (Fukugita et al. 1996) is the most efficient, since (1) this is where the performance of GMOS peaks (Hook et al. 2004), (2) the resolved stellar population will probably be dominated by red giants, and (3) the sky in r' is significantly darker than in redder bands like i'.

The observations are summarized in Table 1. The field locations are illustrated in Figure 1. The inner field (field 1) was placed at the optical edge identified in the Digitized Sky Survey (DSS) to provide continuity with earlier photographic work. While the DSS limit is about 25.5 mag arcsec^{-2} in B_J (3 σ; Corwin 1980), the digitized survey can be displayed at high contrast to reveal a more extended disk. The disk edge is broadly consistent with the photographic limit from photographic amplification (D. F. Malin 2004, private communication). The outer field (field 2) was made to overlap slightly with field 1 in order to check the relative photometric calibration.

The GMOS detector comprises three 2048 × 4608 EEV CCDs arranged in a row, where the long dimensions are edge-butted together (Hook et al. 2004). After 2 × 2 on-chip binning, the pixels are 0.″146 in size. The square field of view in a single GMOS image is 5.′5 on a side. The on-instrument wave front sensor and

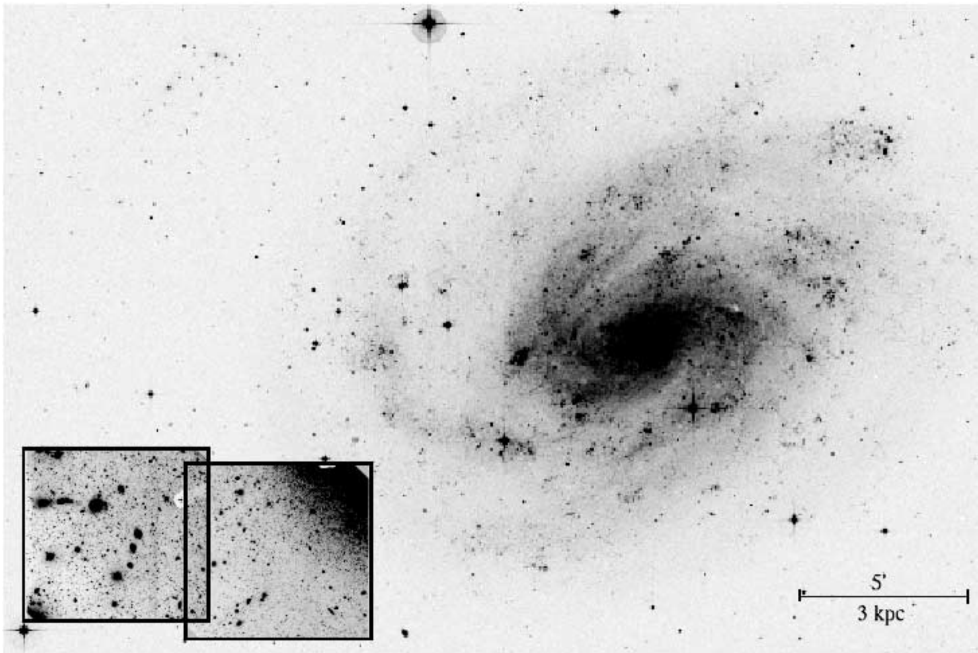

FIG. 1.—Wide-field image ($30' \times 20'$) of NGC 300 from the DSS. (North is at the top and east is left.) The insets show the summed data from the two GMOS outer fields. The GMOS field of view is 5.′5 on a side. The fields are located at a radius of 15.′47 (field 1) and 21.′14 (field 2).

small CCD pixels provided a corrected point-spread function (PSF) of 0.″60 FWHM for field 1 and 0.″63 FWHM for field 2. The PSF was found to be mildly elliptic at about the 10%–15% level. A small PSF is essential for removing contaminating sources in the field. The background levels between exposures varied by no more than 5% generally, and the photometric conditions were excellent.

Each of the fields was observed in 9×900 s dithered exposures. This allowed us to remove cosmic-ray events and edge effects arising from the three edge-butted CCDs. Initially, we used the standard IRAF/Gemini reduction package. The processing pipeline includes bias subtraction and flat fielding (`gireduce`), mosaicking of individual GMOS CCDs into a single reference frame (`gmosaic`), followed by combining the nine dithered exposures (`imcoadd`). The images were then trimmed to the area of common coverage. The final summed images are shown as insets in Figure 1.

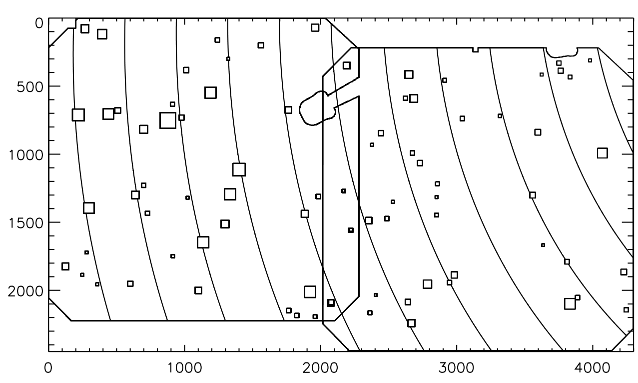

FIG. 2.—Rejection masks for the GMOS fields. The elliptic arcs illustrate how the star counts are binned in azimuth. The major axis of the annuli passes through the middle of field 1. For consistency, all radial profiles are presented in terms of the major axis distance from the galactic nucleus (i.e., defined by the major axis radius of the elliptic annulus). The region eclipsed by the on-instrument wave front sensor can be seen in the top right corner of both fields. The (x, y)-axes are in units of CCD pixels.

The FITS data files arrived without field position information in the headers. Our next step was to astrometrically calibrate the summed field images. This was made possible using the GAIA package developed by P. Draper at the University of Durham. We identified 20 stars in each field with known astrometric positions in the United States Naval Observatory (USNO) photographic catalog (Monet et al. 2003).

Once the fields were correctly aligned with respect to each other, we formed a mask for each field in order to reject unwanted pixels. Both masks are shown in Figure 2. We remove bright foreground stars ($r' < 21$), bright galaxies, and pixels that fall in the shadow of the on-instrument wave front sensor. We also trim the outer perimeter of both fields where the signal-to-noise ratio falls off due to the dithering process. The proportion of pixels lost as a function of galactocentric radius is shown in Figure 6*b*, discussed below. The star counts are normalized to the dotted curves in this figure.

5. STELLAR PHOTOMETRY

Fields 1 and 2 were analyzed using the IRAF DAOPHOT package (Stetson 1987; Davis 1994). For each field, catalogs of 3, 4, and 5 σ source detections were produced with the `daofind` routine. For each catalog, preliminary aperture photometry was obtained using the `phot` task. The routine `psfselect` was used to select approximately the 100 brightest stars, which were then inspected visually. Isolated stars (i.e., without bright neighbors) that were not saturated were chosen for PSF stars. There were about 15 such stars in each field, and they were used as input for the task `psf`, which iteratively computes the PSF model for both fields. Finally, the task `allstar` was run to simultaneously fit this model to stars from the `daofind` catalogs and determine their photometry. The task DAOPHOT identified and returned fitted parameters for 15,671 and 4468 sources in fields 1 and 2, respectively; these numbers dropped to 15,390 and 4291 sources after trimming the field edges.

We examined the residual maps produced by `allstar` to evaluate PSF subtraction with different thresholds. In general, the residuals were slightly cleaner for field 1 when compared

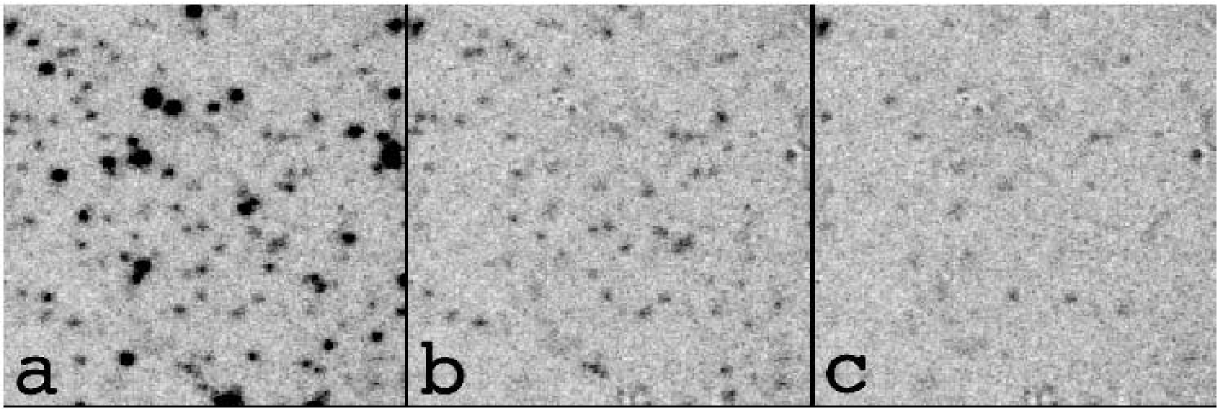

FIG. 3.—A $25'' \times 25''$ subset from the center of field 1 to demonstrate the quality of the DAOPHOT photometric analysis. The images show (*a*) before source subtraction, (*b*) with 5 σ sources subtracted, and (*c*) with 3 σ sources subtracted. The PSF is mildly elliptic (10%–15%) and 0.60″ along the long axis.

with field 2, but for both fields the residuals were less than 1% of the total source flux. In Figure 3, we show a small region from field 1 before subtraction, after subtracting sources above 5 σ, and after subtracting sources above 3 σ. The excellent photometry and source subtraction is evident.

The photometric calibrations were established with two Landolt fields (see Table 1), for which there were half a dozen useful stars in each field (Landolt 1992). The equivalent AB magnitude zero point for a single photoelectron was determined to be $m_{r'} = 28.20$, i.e., 0.1 mag fainter than what is quoted at the Gemini GMOS Web site. The photometric standards showed that the photometry was better than 0.04 mag from night to night and better than 0.02 mag in consecutive exposures.

In Figure 4, we show the magnitude distribution of detected sources found with DAOPHOT. Our catalog is complete to $r' = 27.0$ (3 σ), $r' = 26.7$ (4 σ), and $r' = 26.3$ (5 σ). For comparison, the expected GMOS performance can be assessed with the Web-based calculator,[1] with fair agreement. Our calculation assumes a G5 III spectrum. For 50 percentile observing conditions, an $R_C = 26$ point source in the r' filter requires 8100 s (9×15 minute dithered exposures) for a 5 σ detection. The conversion from R_C to r' is given at the end of this section.

Figure 4 therefore establishes that the observations were undertaken in better than 50 percentile conditions. As a further check on the integrity of our data, the star counts in the overlap region between fields 1 and 2 were compared. We find 10% more stars in field 1 compared to field 2, which is broadly consistent with the higher average background and slightly degraded seeing in the outer field. As we stressed earlier, the PSF subtraction was cleaner for field 1 compared to field 2, and this may contribute to the difference. The magnitude offset between field 1 and field 2 was less than 0.04 mag and consistent with measurements from the Landolt standards. The uniformity between fields is evident from Figure 5.

It is convenient to establish a correction from r' to R_C for two reasons. Most surface brightness profiles published to date are measured in traditional Johnson-Cousins bands (e.g., Kregel et al. 2002). Second, in § 6, we correct the star counts for the background contribution due to distant galaxies. Again, galaxy count surveys to date are quoted in traditional bands (e.g., Metcalfe et al. 2001). Girardi et al. (2002, 2004) derive the requisite transformation from stellar atmospheric models. In the temperature range 4000–10,000 K, $r' - R_C$ changes from about 0.3 to 0.15, with a stronger dependence for cool stars. This compares favorably with

[1] See http://www.gemini.edu/sciops/instruments/instrumentITCIndex.html.

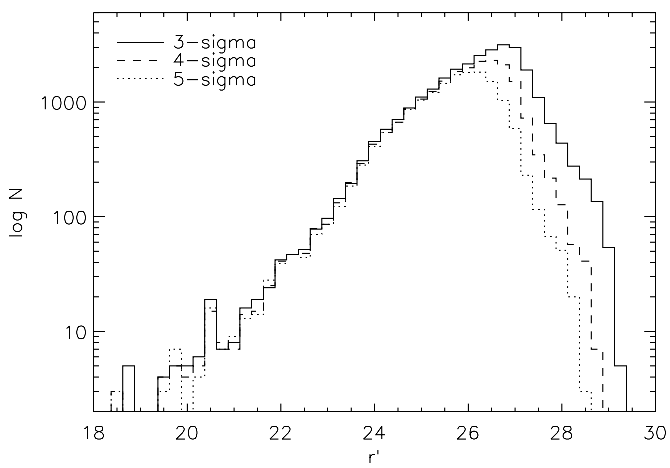

FIG. 4.—The r' magnitude distribution for all sources detected by DAOPHOT. The three curves are from the (*top*) 3 σ catalog, (*middle*) 4 σ catalog, and (*bottom*) 5 σ catalog.

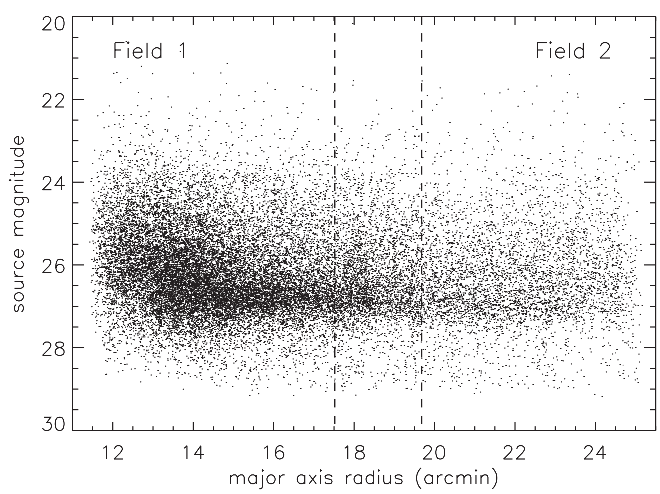

FIG. 5.—Derived r' magnitude in DAOPHOT for all fitted sources as a function of major axis radius. The decline in source counts as a function of radius is evident. Note the incompleteness at 12′ due to crowding in the bright inner disk. Note also the excellent photometric consistency of the data between fields 1 and 2.

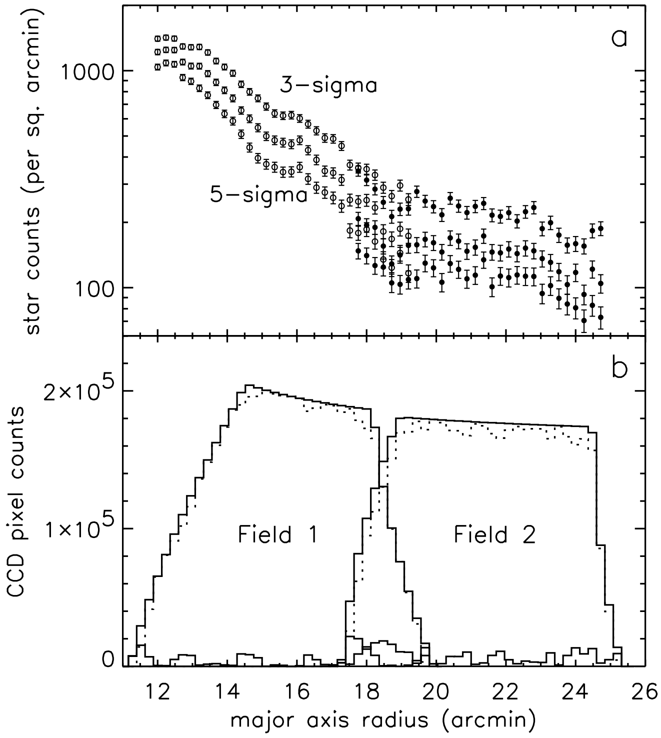

FIG. 6.—(*a*) Source counts per arcmin^2 as a function of radius in the outer GMOS fields for (*top*) 3 σ, (*middle*) 4 σ, and (*bottom*) 5 σ detections. The radial binning is performed in projected elliptic annuli with 100 pixels width (14.″6). The background galaxy counts have not been removed. The error bars are given by $1/N^{1/2}$, where N is the number of stars measured within the annular bin. (*b*) Upper solid histograms show the total number of CCD pixels per radial bin in fields 1 and 2. The lower solid curves show the number of pixels rejected by the mask in Fig. 2. The dotted curves show the impact of the rejected pixels on two upper curves.

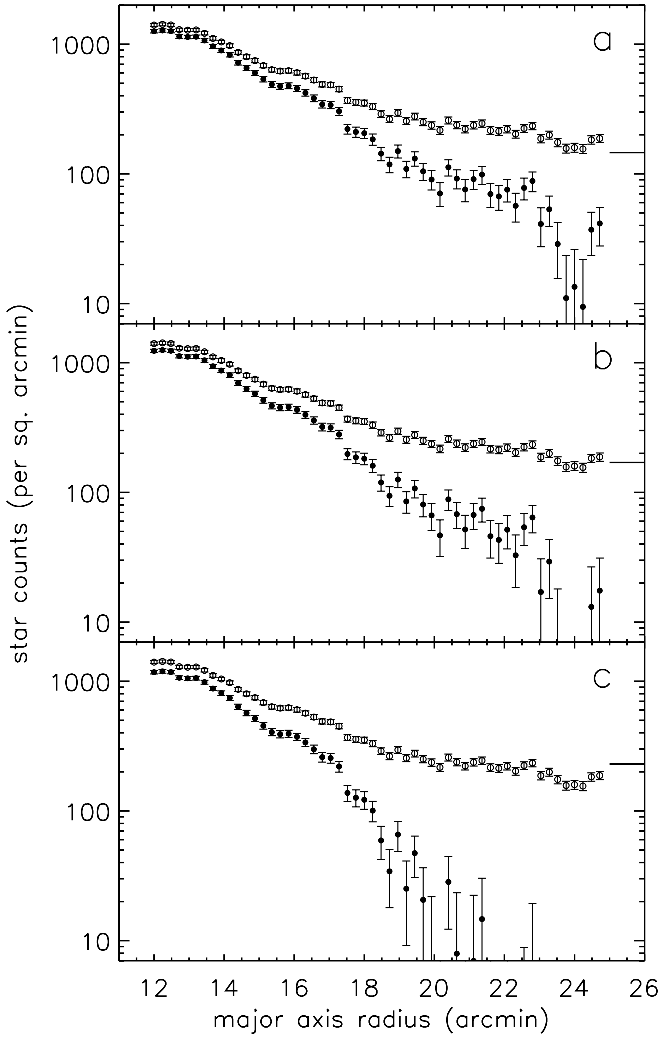

FIG. 7.—Star counts as a function of major axis radius for the 3 σ detections. The counts in the overlap regions have been averaged. We show the counts after subtracting three different background galaxy count levels indicated by the horizontal line: (*a*) predicted counts from averaged Hubble Deep Fields; (*b*) average source counts in the outer eight radial bins (annular width of 800 pixels), assuming that all sources are galaxies; and (*c*) an artificially high background from assuming that all detections in the range 20′–24′ are background galaxies. In each case, the background level is shown by a solid line. The error bars are discussed in the caption for Fig. 6.

Fukugita et al. (1996), who find $r' - R_C = 0.16(V_C - R_C) + 0.13$ such that for stars with $V_C - R_C$ colors of 0.2–0.7, $r' - R_C$ lies in the range 0.16–0.24. Thus, to a good approximation, we can convert our magnitude system to R_C using $r' - R_C = 0.2$.

6. RESULTS

Previous studies have shown that the slope of the radial light distribution of some disks becomes abruptly steeper at an outer break radius (e.g., Pohlen et al. 2002; Kregel et al. 2002); the reason for this break is not known. We now seek to establish whether the stellar disk truncates rapidly beyond the break or extends faintly into the H I disk. Both outcomes have implications for how most of the baryons must have settled during dissipation.

We derive the radial profile of NGC 300 from the catalog of fitted stars. The center of the galaxy was taken from the NASA/IPAC Extragalactic Database (NED). Since the disk is inclined, we need to define elliptic annuli; each annulus has a radial (annular) thickness of 100 pixels. The form of the annuli is illustrated in Figure 2, for which we adopt a position angle P.A. = 110° and inclination $i = 42°$ (Kim et al. 2004). The angle subtended by our fields on the sky is 33° with respect to the nucleus; this translates to 43° projected onto the plane of the disk, or about an eighth of the total azimuthal extent. Note that the disk major axis passes through the middle of field 1.

In Figure 6*a*, we show the radial profile in NGC 300 derived from our source counts *prior to removal of the background galaxy counts.* The form of the profile is essentially identical for the 3, 4, and 5 σ catalogs. The radial profile is normalized by keeping track of the number of pixels in each annular bin. In Figure 6*b*, we see that a typical bin has almost 200,000 pixels. The top-hat distributions are similar in form and overlap at 18.′5. The combined distribution gives uniform coverage from about 12.′5 out to 24.′5. The dotted lines indicate the small corrections required for pixels that are masked out due to bright foreground stars, bright galaxies, and so on (see Fig. 2 and § 4). The star counts are normalized to the dotted curves in this figure.

In Figure 6*a*, there is a gentle transition at 19′ (11.4 kpc), where the profile appears to flatten off. The transition is somewhat emphasized by the nature of the loglinear axes traditional for this field. This happens to fall in the overlap region between fields 1 and 2, as we show in Figure 6*b*. However, the change in slope is not an artifact of joining two data sets, since the form of the transition is identical in both fields. The transition is an artifact of a faint background galaxy population observed through the outer disk of NGC 300.

In order to derive the intrinsic surface brightness profile for NGC 300, we need to remove the background galaxy counts. In Figure 7, we show three possible levels for background subtraction.

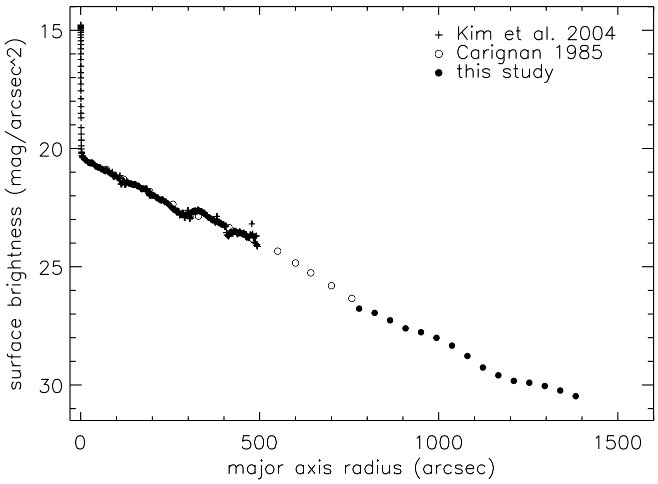

FIG. 8.—Observed r' surface brightness profile of NGC 300 derived *directly* from the star counts. The inner plus signs are taken from Kim et al. (2004): these are *I*-band measurements shifted downward by 0.5 mag. The open circles are taken from the B_J photographic measurements of Carignan (1985) and are shifted upward by 1.1 mag. The GMOS data points are derived from the 3 σ source catalog presented in Fig. 7*b*. After correcting for incompleteness (-0.65 mag) and inclination (+0.33 mag), we obtain the intrinsic surface brightness profile (see § 6); this amounts to shifting all points upward by 0.32 mag.

In Figure 7*a*, we take the average galaxy counts from the Hubble Deep Fields as derived by Metcalfe et al. (2001), where we have taken $r' - R_{\rm C} = 0.2$ (see § 5). Figure 7*b* takes the outer third of field 2 to define the background counts. This is 10% higher than the averaged Hubble Deep Field counts. Given that the expected variance in a 5.′5 field down to $r' = 27$ can be as high as 15% from field to field, this would not be unexpected. The difference in counts between the Hubble Deep Fields when integrated down to $r' = 27$ is about 15% (N. Metcalfe 2004, private communication).

For Figures 7*a* and 7*b*, the key implication is that the disk extends to at least 24′ ($2.2R_{25}$), close to 10 optical scale lengths for this low-luminosity galaxy. It is possible to remove the transition at 18.′5 completely with a background level that is 100% higher than the Hubble Deep Field counts. This outcome is presented in Figure 7*c*. In contrast to Figures 7*a* and 7*b*, the interpretation here would be very different. The disk now appears to truncate very sharply at 18′, or about 50% farther out in radius than the Holmberg radius. Such a cutoff corresponds to about six optical scale lengths, although note that the disk is still detected to $1.9R_{25}$. While we consider this high background level to be unlikely, it cannot be ruled out until more of the outer perimeter of NGC 300 has been mapped under similar observing conditions.

We are not able to separate faint stars from faint background galaxies using the GMOS images. We attempted to separate these with SExtractor, but most of the sources identified as galaxies could not be distinguished from stars convolved with the mildly elliptic PSF. We therefore make the basic assumption that stars and galaxies have the same magnitude distribution in the range $r' = 23$–27. We can then directly convert the magnitudes and number counts in Figure 7*b* to a mean stellar surface brightness as a function of radius.

In Figure 8, photometric data for NGC 300 are superimposed from three sources: (1) Carignan's photographic measurements in $B_{\rm J}$, (2) *I*-band measurements from Kim et al. (2004), and (3) our new GMOS r' measurements. The r' stellar surface brightness profile is derived from the 3 σ catalog presented in Figure 7*b* after background subtraction. Note that this profile reaches exceedingly faint levels of $\mu_{r'} = 30.5$ mag arcsec^{-2} (at 2 σ when averaged over the last two bins in Fig. 7*b*).

We have offset Kim's measurements downward by 0.5 mag ($r' - I = 0.5$) and Carignan's measurements upward by 1.1 mag ($B_{\rm J} - r' = 1.1$). Our population synthesis model in Figure 9 indicates that an appropriate correction is $B_{\rm J} - r' = 1.4$–1.5.

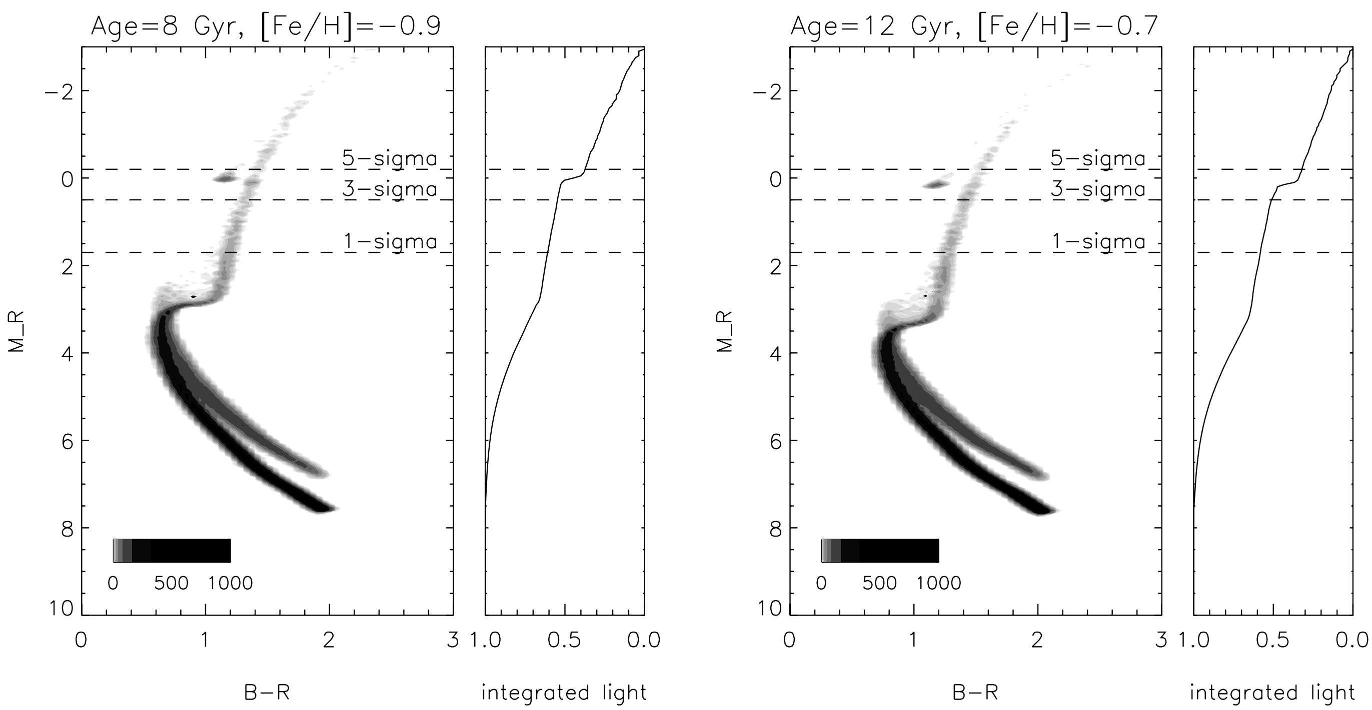

FIG. 9.—Color-magnitude diagram for a stellar population with (*left*) mean age 8 Gyr and [Fe/H] = −0.9 and (*right*) mean age 12 Gyr and [Fe/H] = −0.7. The intrinsic stellar brightness reached by our data is indicated by the horizontal dashed lines for 1, 3, and 5 σ detections. The right figure of each panel shows the fraction of received light from the stellar population above our threshold level. The gray scale indicates the number of stars used in the simulation.

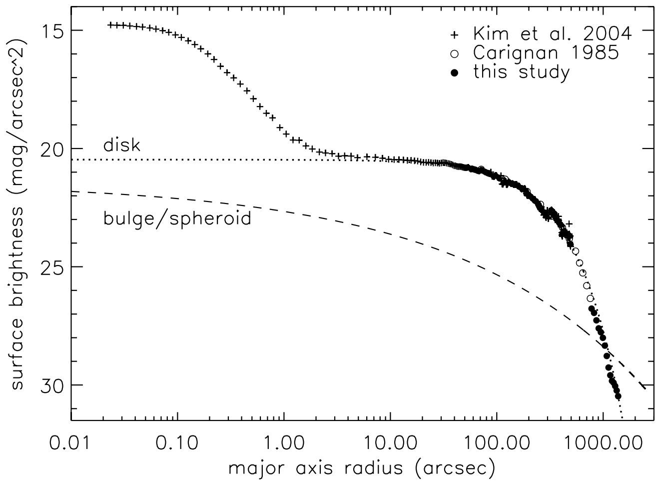

FIG. 10.—The r' surface brightness profile of NGC 300 presented in log radius to emphasize the contribution of the different fitted components. The data points are described in Fig. 8. The continuous curves are the different fitted components, for which the functional forms are given in Kim et al. (2004). The model for the core is not shown.

After applying our correction for stellar incompleteness below, we cannot account for the 0.3 mag offset with respect to Carignan's data; this discrepancy was also noted by Kim et al. when they compared their data with Carignan (1985).

In Figure 10, the logarithmic axes emphasize the different fitted components for the stellar core, the bulge, and the disk. The fitting procedure is described by Kim et al. (2004). Roughly speaking, the data conform to an exponential disk out to 24′. The substructure along the curve may be indicative of our restricted azimuthal coverage. The bulge cannot be strongly constrained in Kim's fitting. However, our figure does make the point that there is *no* compelling evidence for a transition from disk to bulge or halo stars at the outermost observed extent.

The fraction of missing light was estimated from a theoretical color-magnitude diagram derived from the StarFISH code (Harris & Zaritsky 2001). In our models, we explore two possibilities: (1) an intermediate-age 8 Gyr stellar disk with $[\mathrm{Fe/H}] = -0.87$, consistent with the metallicity derived from the red giant population (Tikhonov et al. 2005); and (2) an old 12 Gyr disk with metallicity $[\mathrm{Fe/H}] = -0.7$, comparable to the thick disk of the Galaxy. We specify a Salpeter initial mass function and generate 10^5 stars for each model. The mass function uses a (minimum, maximum) stellar mass of (0.1, 100) $M_\odot$ and a binary fraction of 25%.[2]

The resulting color-magnitude diagrams are shown in Figure 9. Note that the models predict that the GMOS data recover (1) 54.6% and (2) 55.8% of the total light at our 3 σ threshold. Therefore, we estimate our completeness at 55% in the r' images. This would indicate that our surface brightness profile in Figures 8 and 10 should be shifted upward by -0.65 mag in order to correct for the missing light. (We do not attempt to correct for the internal dust extinction.) However, we note that the galaxy inclination ($i = 42°$) renders the surface brightness profile brighter by about -0.32 mag. Therefore, the true upward correction is expected to be -0.33 mag.

With our derived conversion from r' to R_C (§ 6), this indicates that the GMOS data reach down to an effective surface brightness of $\mu_{R_\mathrm{C}} = 30.3$ mag arcsec^{-2}. The color-magnitude diagram simulations in Figure 10 predict an outer disk color $B - I \approx 1.7$. The equivalent surface brightness in B reached by the GMOS data is at the level of $\mu_B = 32$ mag arcsec^{-2}. These are levels that cannot be reached reliably in diffuse light imaging, as we discuss in the Appendix.

[2] The adopted isochrones are taken from http://www.te.astro.it/BASTI (Pietrinferni et al. 2004).

7. DISCUSSION

Our data clearly reveal the presence of a faint stellar disk out to a radius of at least 24′ (14.4 kpc), or about 10 disk scale lengths. Our data extend far beyond the surface photometry of Kim et al. (2004) and show that the disk remains exponential to the radial limits of our counts. There is no evidence for a break in our data, which cover an angular wedge of about 45° within the deprojected disk—the stellar surface brightness is well described by an exponential over almost 10 scale lengths. There is no evidence of a bulge or a halo component.

Indeed, in three wide-field photometric studies of NGC 300, there is no compelling evidence for a break radius in the galaxy luminosity profile (de Vaucouleurs & Page 1962; Carignan 1985; Kim et al. 2004). Carignan (1985, Fig. 5) traces the light in a deep UK Schmidt plate out to $\mu_B = 27.5$ mag arcsec^{-2} at $r = 12\farcm5$. While there may be a hint at a break in Carignan's Figure 14 at about 10′, his earlier figures demonstrate quite different structure when the galaxy is split into two halves.

Since our stellar counts extend to the outer H I disk, it is important to consider the possible effects of a warped stellar disk. Puche et al. (1990) find evidence for a warp in the H I disk beyond 10′, but this does not necessarily indicate that the stellar disk is warped in the same way, if at all (e.g., Garcia-Ruiz et al. 2002). Dramatic stellar warps, which are rarely observed, are most often associated with strong galaxy interactions. There is no obvious interacting companion observed in the vicinity of NGC 300. A weak stellar warp may exist, and its effect would be to slow the radial decline in the stellar luminosity profile. However, there is no such effect evident in either Figures 7 or 10.

The surface brightness of the outer disk of NGC 300 extends smoothly down to at least 30r' mag arcsec^{-2}, which corresponds to a stellar surface density of order 0.01 $M_\odot$ pc^{-2}. To the best of our knowledge, such an extended and very diffuse population of stars has not been seen before. What is its origin?

A key issue is just how far the H I disk extends. Puche et al. (1990) have mapped the outer disk in NGC 300 and detect H I out to 32′, beyond the extent of the newly established optical disk. The H I surface density profile is roughly constant at 0.5–1 $M_\odot$ pc^{-2} in the outer disk. The surface density profile of the optical disk falls with radius and is roughly comparable to the H I at the Holmberg radius, assuming $M/L_R = 1$. Beyond here, the optical surface density falls by a factor of 100 at a radius of 20′ or more.

The existence of stars at such low surface densities is difficult to understand in the conventional picture. How does a spiral density wave initiate and propagate—if this is indeed what triggered star formation in the outer disk—in such a rarefied medium?

The Q criterion is often used to establish whether a disk is unstable to axisymmetric modes, viz.,

$$Q = \frac{\sigma\kappa}{3.36 G\Sigma}, \tag{1}$$

where σ is the internal dispersion of the H I gas, which stabilizes the disk on small scales (up to the radius of the Jeans mass). On larger scales, the disk is stabilized by differential rotation, which is embodied by κ, the epicyclic frequency of the disk. In contrast, the disk is destabilized by its own surface density, Σ. The disk is locally stable against axisymmetric modes if Q is substantially above unity.

We derive $\kappa(r)$ and $\Sigma(r)$ from the data of Puche et al. (1990) and assume $\sigma = 5$ km s^{-1} in the outer disk. We thus find that Q is everywhere greater than 5 ± 2 beyond $10'$, which would appear to argue against star formation and the existence of spiral density waves here.

However, the observations of Puche et al. (1990) not only show that the H I extends well beyond the extent of our stellar disk but also reveal well-defined, tightly wound spiral structure in the H I that is particularly prominent in the southeast at $20'$. While this spiral structure is difficult to explain, it is interesting that H I spiral arms are increasingly observed in the outer parts of disk galaxies (T. A. Oosterloo 2004, private communication; Bureau et al. 1999; Quillen & Pickering 1997). Bureau et al. found a similar problem for the H I disk of NGC 2915, which also shows marked spiral structure at a very large radius; they invoked the effect of a tumbling triaxial halo potential to drive the spiral structure in this apparently stable outer disk.

It is known from photometric imaging studies (e.g., de Jong 1996) that most Hubble types have color gradients from the center outward, which arise from (1) the decreasing dust content, (2) declining stellar abundances, and (3) changing stellar populations due to radial variations in star formation history. The general trend is that disks become progressively bluer at larger radii, and this has been ascribed to the stellar population becoming younger on average and progressively more metal-poor (de Jong 1996).

However, the inference that the stellar populations become progressively younger with radius contrasts with what we know from recent stellar photometry of the outermost reaches of nearby galaxies. These studies incorporate high-quality stellar photometry and show, by comparison with well-calibrated globular cluster data, that the outer giant populations are metal-poor and old. Recent examples include the outer disks of M33 (Galleti et al. 2004) and M31 (Ferguson & Johnson 2001).

The data for NGC 300 are limited at present, but Tikhonov et al. (2005) find that metal-poor ($[\mathrm{Fe/H}] = -0.87$) giants dominate the light at large radius, and these are most likely to be old. We note that Tikhonov et al. attribute various regions of NGC 300 to the thick disk or to the halo, which is difficult to do in a relatively face-on galaxy. One can really only rely on indirect arguments based on our Galaxy, but these are very unreliable. For example, their outermost field (S3) corresponds to a deprojected radius of about 11 kpc, or roughly six scale lengths. In our Galaxy, this corresponds to about 20 kpc, where we know nothing about the stellar disk at the present time.

So is the outer disk in NGC 300 young or old? When one considers the effects of changing extinction and metallicity, a moderately blue outer disk does not necessarily indicate a younger stellar population. (Galleti et al. [2004] discuss how age and metallicity effects can be disentangled in outer disk/halo observations.) Within the context of cold dark matter models, the answer to this question has key implications for the formation scenario for the outer disk (e.g., Ferguson & Johnson 2001).

If follow-up measurements reveal that the outer disk is moderately young, we would expect to find evidence of spiral density waves in the stellar population even at the implied large radii (>12 kpc), although these spiral arms may be moderately diffuse and hard to recognize. As mentioned above, there is clear evidence of spirality in the outer H I disk. If stars are forming today, it may be that the outer H I disk largely comprises cold, compact clouds with internal dispersions lower ($\lesssim 1$ km s^{-1}) than those that one normally associates with beam-averaged observations of outer disks (~ 5 km s^{-1}). If the H I gas was to cool to 100 K and nonthermal (e.g., turbulent) velocities were $\lesssim 1$ km s^{-1}, the Q criterion could be as low as unity. Such clouds would be gravitationally unstable today, and the outer disk would have a moderately young stellar component. But we stress that to our knowledge, the H I velocity dispersion has not been measured in distinct clouds in the outer disk of NGC 300.

If new measurements reveal that the outer disk is old, then the current high value of Q here may simply reflect that the H I has been largely used up today but that there was a time ~ 10 Gyr ago ($z \sim 1$) when there was far more gas than we observe today. If our assumption of the cloud dispersion velocity still holds, this would have the effect of raising the surface density of the disk and lowering the Q parameter to the point at which local instabilities induce star formation.

Hydrogen in the outermost reaches of galaxies may be evidence for gas accretion, either from gas settling onto the dark halo (cold accretion) or from a galaxy merger event (hot accretion). If the material in the slow warp in NGC 300 is the result of gas accretion to the outer disk, it is plausible that the settling process produced low levels of star formation. An example of such a process is dramatically illustrated by the gas disk settling within the giant elliptical galaxy NGC 5128, where a young blue population is clearly evident (Graham 1979; Bland et al. 1987).

But how does an accretion process succeed in maintaining the continuity of the exponential disk? This is particularly puzzling when the surface brightness distribution is contrasted with that of most other spiral galaxies, which show a clear break in their light distribution at 3–5 radial scale lengths. Could the Lin-Pringle viscous evolution of a star-forming disk explain the persistence of the exponential disk of NGC 300 to 10 or more scale lengths?

Another possibility is that the stars were scattered from the inner disk. Recent N-body simulations of disk evolution indicate that radial mixing is strong (Sellwood & Preto 2002). A single spiral wave near corotation can perturb the angular momentum of a star by $\sim 20\%$, moving it either inward or outward by several kiloparsecs (Sellwood & Kosowsky 2002). This process could help to wash out any stellar disk edge, but it is difficult to see how this explains the very extensive stellar disk, with a simple exponential density profile, observed here.

J. B. H. would like to dedicate this work to his brother Simon, who died in 2004 December. We thank the staff of the Gemini Observatory for their tireless efforts and their pursuit of excellence. M. V. was supported by an Anglo-Australian Observatory Student Fellowship in the austral winter of 2004. B. T. D. was supported in part by National Science Foundation grant AST 99-88126. We are grateful to Laura Dunn for her help with running the StarFISH code and to the referee for a careful examination of this paper. The observations presented here were made with the Gemini Multi-Object Spectrograph under program GS-2003B-Q-2. The Gemini Observatory is operated by the Association of Universities for Research in Astronomy, Inc., under a cooperative agreement with the National Science Foundation on behalf of the Gemini partnership: the National Science Foundation (United States), the Particle Physics and Astronomy Research Council (United Kingdom), the National Research Council (Canada), Comisión Nacional de Investigación Científica y Tecnológica (Chile), the Australian Research Council (Australia), Conselho Nacional de Pesquisa Científica e Tecnológica (Brazil), and Consejo Nacional de Investigaciones Científicas y Técnicas (Argentina).

APPENDIX

STARLIGHT SCATTERED BY DUST IN THE OUTER DISK

In our study, we reach an effective surface brightness of $\mu_{r'} = 30.5$ mag arcsec^{-2} (2 σ). This level is exceedingly faint in the sense that the equivalent surface brightness in B or V is fainter than 32 mag arcsec^{-2} for an old stellar population. This raises an important question: is there a practical limit to galaxy photometry? Here we demonstrate that, in principle, the metal-poor outer H I envelope has a sufficient column of dust to scatter detectable levels of starlight from the optical disk. Thus, we propose that only star counts can reliably trace luminosity profiles in galaxies at this faint level or even fainter.

Let us consider a disk with inclination angle i. Starlight from the inner regions of the galaxy will illuminate the dust grains, resulting in scattering. Consider a region in the galaxy where the H nucleon column density normal to the disk is $N_{\rm H}$. If we approximate the illuminating starlight as due to a point source at a distance D with luminosity L_ν located at the galactic center, then the dust grains at a radial distance r from the galactic center will result in scattered intensity I_ν, where

$$I_\nu = \frac{L_\nu}{4\pi r^2}\frac{N_{\rm H}}{\cos i}F_X(\lambda,\ \Theta). \tag{A1}$$

The scattering phase function can be written

$$F_X(\lambda,\ \Theta) \equiv \sum_j \frac{n_j}{n_{\rm H}}\left(\frac{d\sigma}{d\Omega}\right)_{j,\lambda}, \tag{A2}$$

for which $(d\sigma/d\Omega)_j$ is the differential scattering cross section for grain type j at wavelength λ and scattering angle Θ_s and $n_j/n_{\rm H}$ is the number of grains of type j per H nucleon. Equation (A1) can be rewritten as

$$\frac{I_\nu}{29\ \text{mag arcsec}^{-2}} = \frac{1}{\cos i}\left(\frac{r/D}{\text{arcsec}}\right)^{-2}\left(\frac{N_{\rm H}}{10^{18}\ \text{cm}^{-2}}\right)\left[\frac{F_X(\lambda,\ \Theta_s)}{10^{-24}\ \text{cm}^2\ \text{sr}^{-1}}\right]10^{0.4\left(14-m_{\rm gal}\right)}, \tag{A3}$$

where $m_{\rm gal}$ is the apparent magnitude of the galaxy. For NGC 300, the NED database gives $m_{\rm gal} = 8.95$ in the B band rising to $m_{\rm gal} = 7.5$ in the R band.

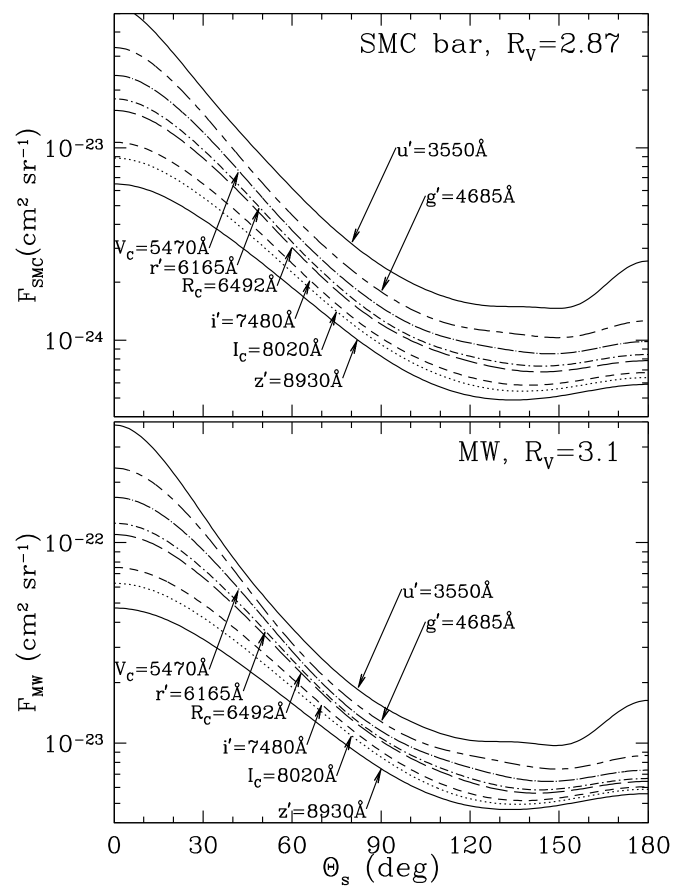

FIG. 11.—$F(\lambda, \Theta)$ or Milky Way dust with $R_V = 3.1$ (*bottom panel*) and SMC bar dust with $R_V = 2.9$ (*top panel*) at selected wavelengths λ (Sloan Digital Sky Survey z', i', r', g', and u' and Cousins $I_{\rm C}$, $R_{\rm C}$, and $V_{\rm C}$), as a function of the scattering angle Θ_s.

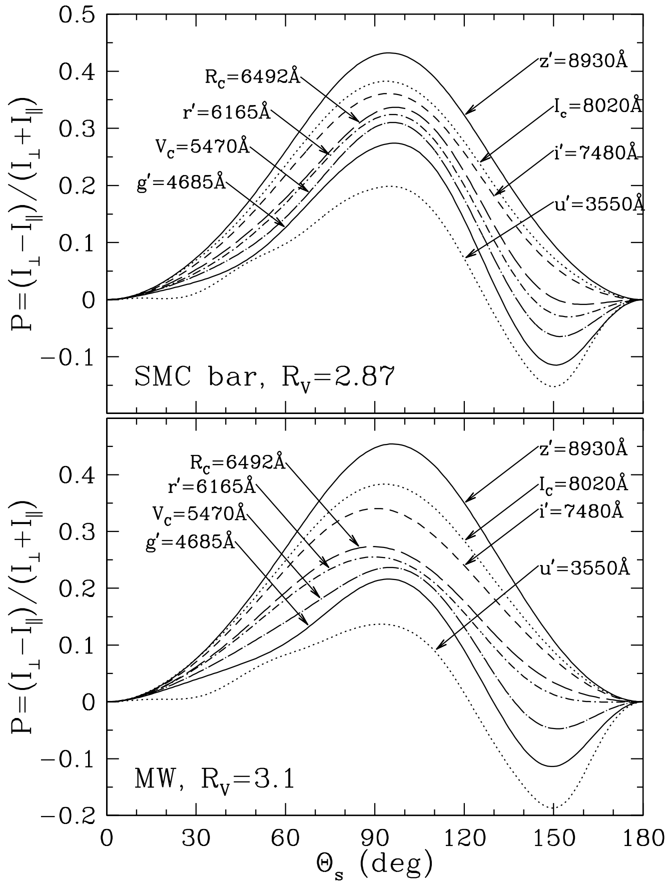

FIG. 12.—Degree of polarization for scattering by Milky Way dust with $R_V = 3.1$ and SMC bar dust with $R_V = 2.9$ at selected wavelengths λ as a function of the scattering angle Θ_s.

If the location in the galaxy is specified by the observed position angle ψ (measured from the minor axis, with $\psi = 0$ corresponding to the side of the galaxy nearest to us) and displacement Θ from the center, then

$$\frac{I_\nu}{29 \text{ mag arcsec}^{-2}} = \frac{\cos i(1 + \tan^2\psi)}{1 + \cos^2 i \tan^2\psi}\left(\frac{\Theta}{\text{arcsec}}\right)^{-2}\left(\frac{N_{\rm H}}{10^{18} \text{ cm}^{-2}}\right)\left[\frac{F_X(\lambda, \Theta_s)}{10^{-24} \text{ cm}^2 \text{ sr}^{-1}}\right]10^{0.4\left(14-m_{\rm gal}\right)}. \tag{A4}$$

The scattering angle Θ_s is related to inclination i and position angle ψ by

$$\Theta_s = \arccos\left(\frac{\sin i}{\sqrt{1 + \cos^2 i \tan^2\psi}}\right), \tag{A5}$$

leading to $\Theta_s = 90°$ for a face-on galaxy ($i = 0$).

Weingartner & Draine (2001) have developed dust models that reproduce the observed wavelength-dependent extinction in the Milky Way, LMC, and SMC. These models are also consistent with the observed infrared and far-infrared emission (Li & Draine 2001, 2002). The scattering properties of these dust models have been calculated by Draine (2003). Figure 11 shows $F(\Theta_s)$ from Draine (2003) at selected wavelengths for Milky Way (MW) dust and SMC dust. Note that $F(\lambda, \Theta_s)$ for the SMC is lower than for the Milky Way by approximately a factor of 10, which is approximately the metallicity of the SMC relative to the solar value. Thus, it seems reasonable to estimate $F_X(\lambda, \Theta_s) \approx (Z/Z_\odot)F_{\rm MW}(\lambda, \Theta_s)$ as an estimate for F_X in another galaxy.

Puche et al. (1990) measured $N(\text{H I}) \approx 9 \times 10^{19}$ cm^{-2} in NGC 300 at 1000″. For the outer disk of NGC 300, the red giant color distribution indicates [Fe/H] $= -0.87$ (Tikhonov et al. 2005); we take $Z/Z_\odot \approx 0.2$ for the gas. Evaluating equation (A3) for a point on the major axis 1000″ from the center, we find $I \approx 31.5$ mag arcsec^{-2}, or about 4% of the stellar surface brightness at this point. Scattered starlight makes a small contribution to the total surface brightness for NGC 300 at $r = 1000''$, but for other cases (e.g., galaxies in which the stellar surface density declines more rapidly) scattered starlight could contribute a larger fraction of the total surface brightness.

Scattered starlight, if present, will be substantially polarized. In Figure 12, we show the degree of linear polarization expected for the scattered light as a function of scattering angle, where we assume that the galactic starlight incident on the dust grains is unpolarized. For a 90° scattering angle (e.g., for a face-on galaxy) the polarization is expected to be ~45% in red light, with smaller values at shorter wavelengths.

In addition to scattering light, dust grains appear to luminesce in the red when illuminated by ultraviolet light (see Witt & Vijh 2004 and references therein). This so-called extended red emission can be comparable in intensity to the scattered starlight in the red.

REFERENCES

Barton, I. J., & Thompson, L. A. 1997, AJ, 114, 655
Bernstein, R., Freedman, W. L., & Madore, B. F. 2002, ApJ, 571, 56
Blair, W. P., & Long, K. S. 1997, ApJS, 108, 261
Bland, J., Taylor, K., & Atherton, P. D. 1987, MNRAS, 228, 595
Brown, T. M., Ferguson, H. C., Smith, E., Kimble, R. A., Sweigart, A. V., Renzini, A., Rich, R. M., & VandenBerg, D. A. 2003, ApJ, 592, L17
Bureau, M., Freeman, K. C., Pfizner, D. W., & Meurer, G. R. 1999, AJ, 118, 2158
Butler, D. J., Martinez-Delgado, D., & Brandner, W. 2004, AJ, 127, 1472
Carignan, C. 1985, ApJS, 58, 107
Corwin, H. G. 1980, MNRAS, 191, 1
Davis, L. E. 1994, A Reference Guide to the IRAF/DAOPHOT Package (Tucson: NOAO)
de Grijs, R., Kregel, M., & Wesson, K. H. 2001, MNRAS, 324, 1074
de Jong, R. S. 1996, A&A, 313, 377
de Vaucouleurs, G., & Capaccioli, M. 1979, ApJS, 40, 699
de Vaucouleurs, G., & Page, J. 1962, ApJ, 136, 107
Draine, B. T. 2003, ApJ, 598, 1017
Ferguson, A. M. N., & Clarke, C. J. 2001, MNRAS, 325, 781
Ferguson, A. M. N., & Johnson, R. A. 2001, ApJ, 559, L13
Freedman, W., et al. 2001, ApJ, 553, 47
Freeman, K. C. 1970, ApJ, 160, 811
Freeman, K. C., & Bland-Hawthorn, J. 2002, ARA&A, 40, 487
Fukugita, M., Ichikawa, T., Gunn, J. E., Doi, M., Shimasaku, K., & Schneider, D. P. 1996, AJ, 111, 1748
Galleti, S., Bellazzini, M., & Ferraro, F. R. 2004, A&A, 423, 925
Garcia-Ruiz, I., Sancisi, R., & Kuijken, K. 2002, A&A, 394, 769
Gieren, W., et al. 2004, AJ, 128, 1167
Girardi, L. 2002, A&A, 391, 195
———. 2004, A&A, 422, 205
Graham, J. A. 1979, ApJ, 232, 60
Haikala, L. K., & Mattila, K. 1995, ApJ, 443, L33
Harris, J., & Zaritsky, D. 2001, ApJS, 136, 25
Hook, I. M., Jørgensen, I., Allington-Smith, J. R., Davies, R. L., Metcalfe, N., Murowinski, R. G., & Crampton, D. 2004, PASP, 116, 425
Jerjen, H., Freeman, K. C., & Binggeli, B. 1998, AJ, 116, 2873
Kim, S. C., Sung, H., Park, H. S., & Sung, E.-C. 2004, Chinese J. Astron. Astrophys., 4, 299
Kregel, M., van der Kruit, P. C., & de Grijs, R. 2002, MNRAS, 334, 646
Labbé, I., et al. 2003, ApJ, 591, L95
Landolt, A. 1992, AJ, 104, 340
Li, A., & Draine, B. T. 2001, ApJ, 554, 778
———. 2002, ApJ, 576, 762
Lin, D. N. C., & Pringle, J. E. 1987, ApJ, 320, L87
Maloney, P. R. 1993, ApJ, 414, 41
Maloney, P. R., & Bland-Hawthorn, J. 2001, ApJ, 553, L129
Metcalfe, N., Shanks, T., Campos, A., McCracken, H. J., & Fong, R. 2001, MNRAS, 323, 795
Monet, D., et al. 2003, AJ, 125, 984
Pietrinferni, A., Cassisi, S., Salaris, M., & Castelli, F. 2004, ApJ, 612, 168
Pohlen, M., Dettmar, R.-J., Lütticke, R., & Aronica, G. 2002, A&A, 392, 807
Pohlen, M., Beckman, J. E., Huettemeister, S., Knapen, J. H., Erwin, P., & Dettmar, R.-J. 2004, in Penetrating Bars through Masks of Cosmic Dust: The Hubble Tuning Fork Strikes a New Note, ed. D. L. Block et al. (New York: Springer), 713
Pritchet, C. J., & van den Bergh, S. 1994, AJ, 107, 1730
Puche, D., Carignan, C., & Bosma, A. 1990, AJ, 100, 1468
Quillen, A. C., & Pickering, T. E. 1997, AJ, 113, 2075
Reynolds, R. J. 1992, ApJ, 392, L35
Schlegel, D. J., Finkbeiner, D. P., & Davis, M. 1998, ApJ, 500, 525
Sellwood, J. A., & Kosowsky, A. 2002, in ASP Conf. Ser. 273, The Dynamics, Structure, and History of Galaxies, ed. G. Da Costa & H. Jerjen (San Francisco: ASP), 243
Sellwood, J. A., & Preto, M. 2002, in ASP Conf. Ser. 275, Disks of Galaxies: Kinematics, Dynamics, and Perturbations, ed. E. Athanassoula, A. Bosma, & R. Mujica (San Francisco: ASP), 281
Stetson, P. B. 1987, PASP, 99, 191
Tikhonov, N. A., Galazutdinova, O. A., & Drozdovsky, I. O. 2005, A&A, 431, 127
van der Kruit, P. 1979, A&AS, 38, 15
———. 1987, A&A, 173, 59
Weiner, B. J., Williams, T. B., van Gorkom, J. H., & Sellwood, J. A. 2001, ApJ, 546, 916
Weingartner, J. C., & Draine, B. T. 2001, ApJ, 548, 296
Witt, A. N., & Vijh, U. P. 2004, in ASP Conf. Ser. 309, Astrophysics of Dust, ed. A. N. Witt, G. C. Clayton, & B. T. Draine (San Francisco: ASP), 115